AIAA JOURNAL
Vol. 40, No. 7, July 2002

Acoustic Noise-Source Identification in Aircraft-Based Atmospheric Temperature Measurements

Ronald J. Hugo*
University of Calgary, Calgary, Alberta T2N 1N4, Canada
and
Scott R. Nowlin,† Ila L. Hahn,‡ Frank D. Eaton,§ and Kim A. McCrae¶
U.S. Air Force Research Laboratory, Kirtland Air Force Base, New Mexico 87117

Atmospheric temperature fluctuation data collected from a Grumman Gulfstream II aircraft show features in temperature power spectral density functions that do not follow the expected $-\frac{5}{3}$ slope for homogeneous isotropic turbulence. Spectral analysis techniques show that these features result from the upstream propagation of a nondispersive acoustical wave. The source of the acoustical wave, which appears only at flight altitudes greater than 28,000 ft (8530 m), is attributed to engine acoustics in the form of jet screech where vortical structures interact with a quasi-periodic shock cell structure, both in the jet exhaust. The nature of the acoustical disturbance is shown to be dependent on velocity, with increased velocity resulting in a decrease in jet-screech peak frequency. These results are found to be consistent with those of other researchers investigating jet screech in jet flows.

I. Introduction

OVER a period spanning the past 20 years, personnel in the atmospheric characterization group at the U.S. Air Force Research Laboratory (AFRL) have performed aircraft-based measurements of atmospheric temperature fluctuations in the troposphere and stratosphere.[1−3] The majority of these measurements have been made using 5-μm-diam fine wires operating in the constant-current mode [constant current anemometer (CCA)] as a resistance thermometer. With flight Mach numbers ranging from 0.7 to 0.8, compressibility effects can complicate the procedure by which static temperature measurements are isolated from the measured total temperature. This issue is addressed elsewhere,[4,5] and consequently it will not be considered in this paper. For typical flight speeds of 200 m/s, the thermal inertia of the wire limits the frequency response of the sensor to approximately 400 Hz (Ref. 6). This effect can be evidenced by examining a temperature spectra under conditions of strong turbulence, as shown in Fig. 1, and noting the probe roll off for wave numbers ($k = 2\pi f/U$) greater than 10. The probe roll off results in a departure from the expected $-\frac{5}{3}$ slope in the inertial subrange for isotropic homogeneous turbulence.[7,8]

A -3 slope is sometimes noted under very weak turbulence conditions and is believed to be associated with either transitional laminar free shear flows or with gravity-wave activity.[9] It is also under these weak turbulence conditions that other non-Kolmogorov features appear in the temperature spectra, and their nature depends on the aircraft flown and on the flight Mach number. One example of these non-Kolmogorov features can be seen in the temperature spectra in Fig. 2, collected from a Grumman Gulfstream II aircraft, where a spike/bump feature is seen along with what are labeled as high Mach features. The spike/bump feature was found to appear over a broad range of flight Mach numbers while flying at altitudes above 28,000 ft (8530 m). The high Mach features were found to appear in the data when the aircraft Mach number exceeded approximately 0.78 and were attributed to a shock-induced flow-separation instability that formed on the probe-mount strut once a critical Mach number was reached.[10]

Characteristics similar to the spike/bump feature have been seen in temperature spectra collected from a C-135E aircraft. An example of one of these spectra under weak turbulence conditions is shown in Fig. 3, where a bump feature can be seen. The bump in the C-135E data is noted to have a lower peak amplitude than the Gulfstream II data, and it extends to higher wave numbers, spanning a broader wave-number range.

Given the fact that these spectral features were found to vary with flight Mach number and were dependent on aircraft platform, it was reasonable to assume that their origin was not attributable to atmospheric turbulence. Agreement between the temperature spectra collected on the Gulfstream II (Fig. 2) and jet-noise acoustic spectra collected in the far field of both convergent-divergent and convergent-choked jets by other investigators[11−14] (a characteristic spectra is shown in Fig. 4) strongly suggests that the spike/bump feature is aeroacoustical in nature. A series of flight-test experiments was conducted in order to further substantiate this claim, and the experimental results are presented in this paper. These results also provide the opportunity to compare laboratory-based experimental data, collected by other researchers, with the operational-aircraft data presented in this paper. Such a comparison will be made in the paper.

The paper begins by describing the Gulfstream II aircraft and the associated experimental equipment used to investigate the source of the spike/bump feature. A section describing flight tests used to investigate the spike/bump feature is next presented. This is followed by a section where the spike amplitude and frequency are characterized as a function of flight conditions. The paper ends with a discussion and conclusions section.

II. Experimental Apparatus

As mentioned in the Introduction, the goal of the atmospheric characterization program has been to collect atmospheric temperature fluctuation data in the troposphere and stratosphere. Temperature fluctuations at these altitudes and in the frequency range of interest are low and on the order of milliKelvins. These low signal

Received 16 February 2001; revision received 10 December 2001; accepted for publication 18 December 2001.

*Assistant Professor, Department of Mechanical and Manufacturing Engineering, 2500 University Drive, N.W.

†Capt., U.S. Air Force, Lead Flight Test Engineer, Directed Energy Directorate; currently Capt., U.S. Air Force, Department of Aeronautics, U.S. Air Force Academy, HQ USAFA/DFAN, 2354 Fairchild Drive, 6H39, U.S. Air Force Academy, CO 80840-6222.

‡1st Lt., U.S. Air Force, Flight Test Engineer, Directed Energy Directorate; currently Capt., U.S. Air Force, SMC/MT3S, 185 Discoverer Boulevard, Suite 2512, El Segundo, CA 90245.

§Senior Research Physicist, Directed Energy Directorate.

¶Major, U.S. Air Force, Team Leader, Directed Energy Directorate; currently Lt. Col., U.S. Air Force, MDA/TES, 7100 Defense Pentagon, Washington, DC 20301-7100.

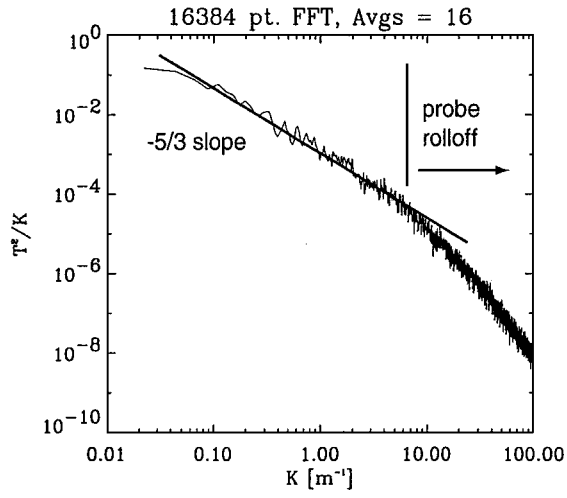

Fig. 1 Temperature spectra: Kolmogorov.

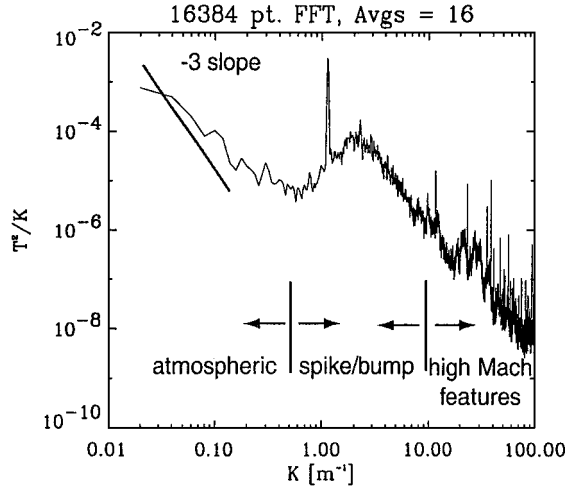

Fig. 2 Temperature spectra: spike-bump on Gulfstream II aircraft.

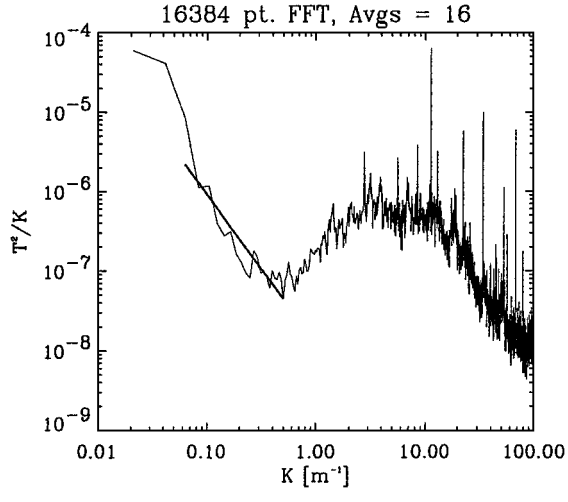

Fig. 3 Bump on C-135E aircraft.

levels have led to the development of a high-gain/low-electronic-noise constant current anemometer system.[3] The normal constant current anemometer sensor suite (described in Ref. 3) was augmented while the experiments presented here were performed and will be described in the following subsections.

Aircraft Description

Data were collected with the constant current anemometer probe mount installed on the side of a Grumman Gulfstream II aircraft (S/N 023), which will be referred to as the GII in this paper. The

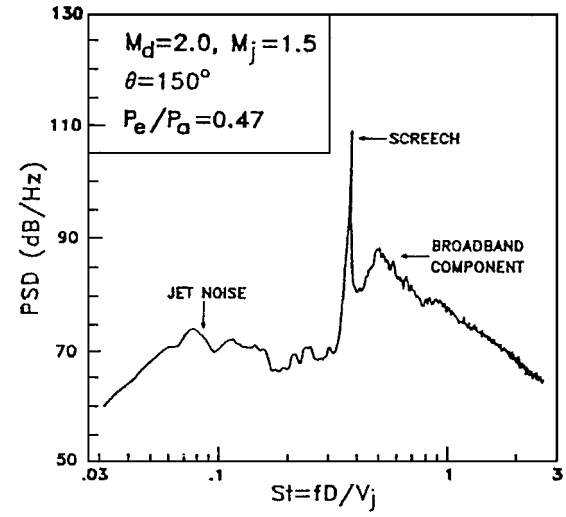

Fig. 4 Typical far-field narrowband shock noise spectrum.[11]

GII was equipped with the radome of a Gulfstream III; otherwise, the aircraft was a standard GII. The probe mount was secured to an existing oval fuselage panel on the lower left side of the fuselage parallel to the front landing gear and below the fuselage's horizontal centerplane.

The GII was equipped with two Rolls–Royce Spey Mk 511-8 turbofan engines. The Spey Mk 511-8 has a two-spool-type axial-flow compressor, consisting of a five-stage low-pressure section and a twelve-stage high-pressure section. The blade passage frequency of the first stage of the low-pressure compressor is 1400 Hz at 50% maximum engine rpm and 2800 Hz at maximum engine rpm. At typical data collection flight speeds of 200 m/s, acoustical noise caused by blade passage frequency would result in spectral energy at wave numbers of $k = 44$ and 88, respectively. It can thus be concluded that blade passage frequency is not the source of the spike in the atmospheric temperature spectra (Fig. 2). The engine's jet exhaust was convergent and of the fixed-area type, 0.55 m in diameter, and was without noise suppression equipment. The engine exhaust plane of the symmetrically opposed turbofan engines is 17.43 m aft of the radome nose and 1.94 m off of the aircraft's centerline.

Anemometer/Probe Mount

The fragile nature of the 5-μm constant current probes led to the development of a protective probe mount by members of the AFRL atmospheric characterization group in the early 1990s. The probe mount protects the anemometer probes during climb out and then extends them once the aircraft is clear of clouds. The probe mount consists of a strut extending perpendicular from the fuselage wall, with two probe arms extending forward from the strut. Heater strips are mounted on either side of each probe arm. They are used to prevent the formation of ice during climb out, and power to the heaters is turned off once clear of clouds. A more detailed description of the probe mount geometry can be found in Ref. 10.

The constant current wire probes are mounted at the upstream tip of the probe arms in either an extended or retracted configuration. The probes used are DISA 55P52s, which consist of two cross wires per probe, meaning that a total of four wires can be extended at any given time. The two probe arms provide a degree of redundancy in the event that an extended set of wires should break as a result of a collision with an airborne particle; the other set of protected (retracted) wires can be extended and used. When extended, the 55P52 sensor is located 2.08 m aft of the nose of the GII and 0.81 m off of the aircraft's centerline.

In addition to the constant current wires, the probe mount has a PCB microphone (MIC 1), Model 103A03, mounted in the end plate of the probe-mount strut (2.74 m aft of nose). A second microphone (MIC 2) was flush mounted in the GII's fuselage wall above and at the same streamwise position as the constant current wires, and a third (MIC 3) was mounted on the fuselage approximately 4

jet-nozzle diameters downstream of the engine-exhaust exit plane along the aircraft centerline (equidistant to both engine exhaust planes). Each microphone signal was fed through a battery-powered signal conditioner, PCB Model 480E09. The microphone signals were used to monitor the engine acoustics and correlate engine noise with the suspected nonatmospheric sources found in the temperature spectra.

Data collected during a typical flight test consisted of four channels of fluctuating total temperature data from the CCA and three channels of microphone data. (In the event of both probes extended, four wires are extended simultaneously.) The data were acquired at 12 kHz (per channel) with a TEAC RD-130TE DAT data recorder, which provided internal antialiasing filters. The data were then transferred to an IBM RS/6000 and processed using Interactive Data Language analysis routines. All spectra presented in this paper were evaluated based on ensembles of 16 nonoverlapped Hanning-windowed 16384 point fast Fourier transforms (FFTs). Aircraft Mach number was logged as a function of time during accelerating flight conditions, along with pressure altitude and atmospheric static temperature by reading cockpit indicators.

III. Noise-Source Identification

Two sets of experiments were performed while identifying the noise source: the first consisted of flying the aircraft at a constant Mach number and pressure altitude, and the second consisted of accelerating the aircraft at a constant pressure altitude.

Constant-Mach-Number Flight Tests

Examples of spectra for the temperature fluctuations and two of the microphone signals collected at a fixed aircraft speed of 230 m/s and an altitude of 41,000 ft (12,500 m) are shown in Figs. 5–7.

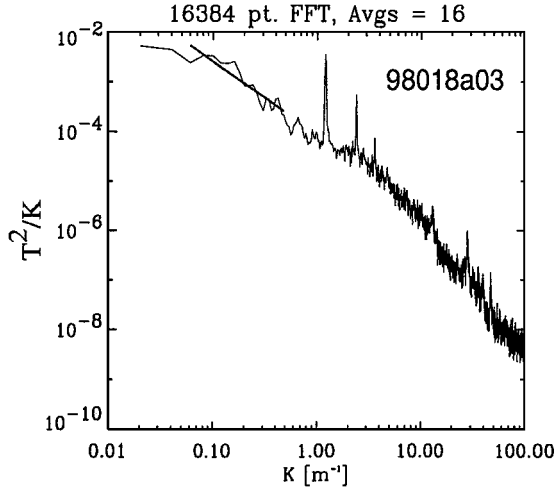

Fig. 5 PSD of CCA channel.

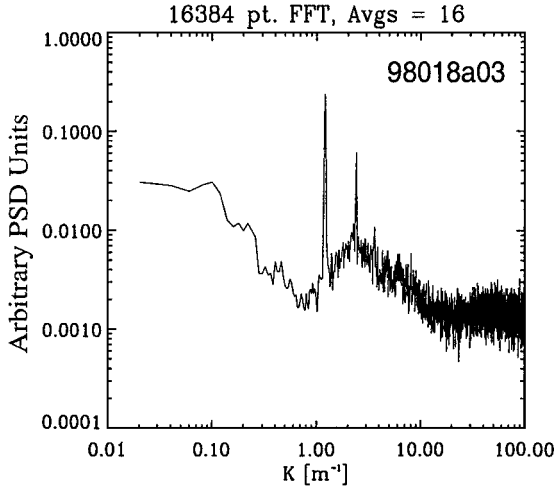

Fig. 6 PSD of forward fuselage microphone (MIC 2).

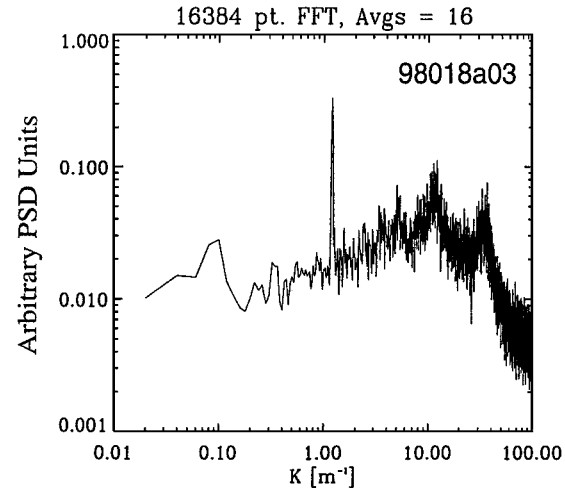

Fig. 7 PSD of aft fuselage microphone (MIC 3).

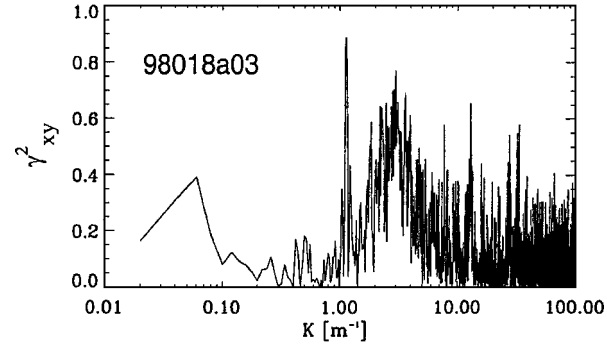

Fig. 8 Coherency function between CCA and forward fuselage microphone (MIC 2).

Comparing the spectra of total temperature fluctuations measured by the constant current wire (Fig. 5) with the spectra for the forward fuselage-mounted microphone (MIC 2 in Fig. 6), it can be seen that the microphone spectra show a similar spike/bump combination over wave-number range $k = 1 \rightarrow 3$, which corresponds to the location of the spikes in the temperature spectra. The spectra of MIC 3, mounted downstream of the engine's nozzle exit plane, are shown in Fig. 7 and also provide evidence of a spike at wave number $k \approx 1.2$ in addition to a higher frequency and broader dual bump.

Further information can be extracted from the signals by computing the coherence function $\gamma_{xy}^2(f)$ between the CCA signal and the fuselage-mounted microphone (MIC 2). The coherence function is defined as[15]

$$\gamma_{xy}^2(f) = \frac{|G_{xy}(f)|^2}{G_{xx}(f)G_{yy}(f)} \tag{1}$$

where G_{xy} represents the cross-spectral density function:

$$G_{xy} = (2/N\Delta t)\left[X_x^* \times X_y\right] \tag{2}$$

and G_{xx} and G_{yy} the autospectral density function given by

$$G_{xx} = (2/N\Delta t)\left[X_x^* \times X_x\right] \tag{3}$$

$$G_{yy} = (2/N\Delta t)\left[X_y^* \times X_y\right] \tag{4}$$

Here X_x represents the complex Fourier transform of signal x and X_x^* its complex conjugate. The N in Eqs. (2–4) represents the number of data points used to compute the FFT and Δt the time interval between consecutive data points.

The results of this calculation are shown in Fig. 8, where the coherence between the total temperature fluctuations and the pressure fluctuations are plotted. The coherence is high at the location of the spike/bump and low otherwise with values mostly below 0.2. The

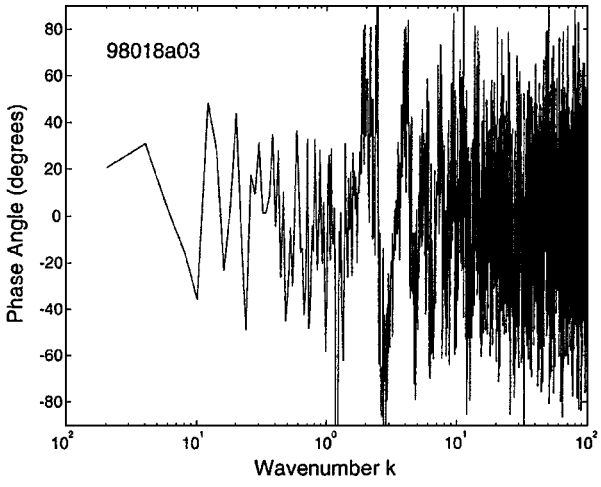

Fig. 9 Phase angle between CCA and MIC 1: log scale.

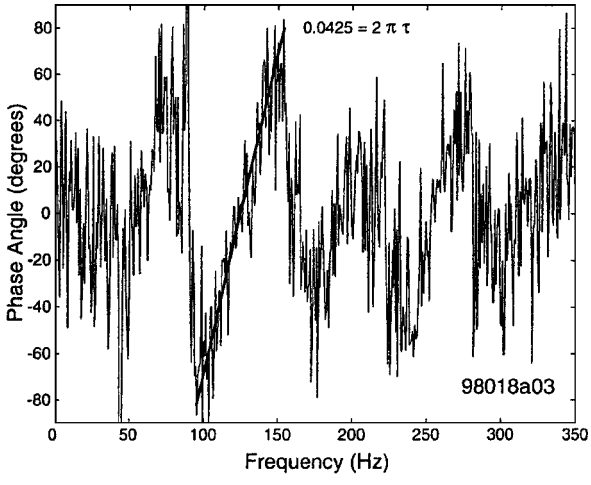

Fig. 10 Phase angle between CCA and MIC 1: linear scale (magnified).

high coherence in the region of the spike/bump implies that, as suspected, the features noted in the temperature spectra are not caused by atmospheric temperature fluctuations but are rather caused by pressure fluctuations.

Figure 9 shows the phase-angle relationship between the CCA signal and the probe-mount microphone plotted as a function of wave number. The region between wave numbers 1 and 10 reveals certain features that when replotted linearly as a function of circular frequency, as done in Fig. 10, show a linear relationship between phase angle and frequency. This type of relationship is indicative of a nondispersive propagating wave.[16,17] Also shown in Fig. 10 is a line denoting the slope of the phase-angle/frequency relationship (expressed in units of radians per hertz). As described in Ref. 17, this slope is equal to $2\pi\tau$ and can be used to determine the time delay τ for the propagating wave to travel between the two sensors, which results in a time delay τ of 6.76×10^{-3} s.

The propagation velocity of an upstream traveling acoustic wave should equal the difference between the speed of sound at flight level ($a = 295.3$ m/s) and the flow speed at the probe mount U_f. The spatial distance between the two sensors is 0.67 m, and consequently this can be divided by τ to determine the wave propagation speed ($U_w = 99.1$ m/s). The flow speed at the probe mount location can be computed to be $U_f = a - U_w = 196.2$ m/s. This implies that the flow speed at the probe mount is 85% the freestream velocity (230.3 m/s). Data pertaining to the external flow velocities on a GII aircraft with the radome of a GIII were not available for this number to be verified; however, given that the probe is mounted just aft of the radome in an accelerating-flow region makes this number plausible.

Both the coherence function and phase relation support the notion that the source of the spike/bump feature in the CCA data is caused by an upstream propagating nondispersive wave that is acoustical in

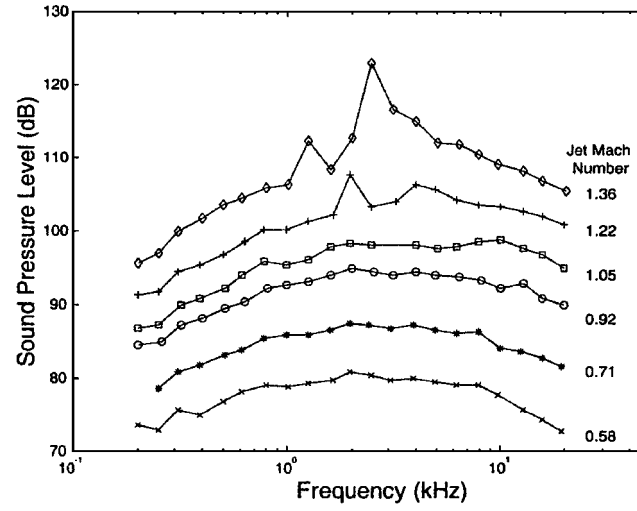

Fig. 11 Jet noise spectra for a convergent nozzle.[18]

nature. As mentioned in the Introduction, the source of this acoustical noise is believed to be aeroacoustic in nature, resulting from the dynamics of the jet exhaust. Similar spike/bump features can be observed in acoustic spectra collected from both convergent-divergent nozzles operating at off-design Mach numbers (Ref. 18 and illustrated in Fig. 11) and from convergent choked jets.[12–14] The latter form of jet flow is present on the GII. It is speculated that the fact that the noise appears in spectra collected at altitudes only above 28,000 ft (8530 m) would correspond to the point at which the jet exhaust becomes choked. Convergent choked jets can issue an underexpanded supersonic jet. The spikes in the spectra are attributed to a jet screech phenomena involving resonant interactions between the jet's vortical structures and a quasi-periodic shock cell structure that develops in the jet stream.

The acoustical disturbance on the GII could be enhanced further by a phase coupling between the twin exhaust plumes. This type of coupling has been reported in the literature[19] for aircraft such as the F-15 and B-1B where the centerline spacing between engines is two nozzle diameters or less. The centerline spacing on the GII is larger at seven nozzle diameters. It is at present unclear whether the observed features in the spectra are being enhanced by a phase coupling.

Accelerating Flight Tests

Accelerating data at a constant pressure altitude provide a means of observing the variability in the acoustical disturbance as a function of flight Mach number. This test was conducted by collecting a six-minute data record as the aircraft was accelerated from a Mach number of 0.52 to 0.84 at an altitude of 39,100 ft (11,918 m). The change in flight Mach number results in a change in the character of the engine acoustics; consequently, accelerating data are inherently nonstationary. An efficient method of examining such data is through a sliding-window FFT. Power spectral density functions (PSDs) for a particular accelerating run were computed using a sliding-window data set where 22 s of data was used to compute an individual PSD (16,384 point FFT and 16 ensemble averages, comprising 262,144 data points in each data set). The next consecutive PSD was then computed by dropping the last 16,384 points from the data set and adding 16,384 new data points to the start of the data set. This resulted in a new PSD for every 1.36 s of new data.

Spectra computed using the CCA signal are shown in Fig. 12 at five different "average" Mach numbers during the accelerating run, starting at Mach 0.52 in the lowest curve and progressing to Mach 0.82 in the uppermost curve. The term "average" Mach number is used as the aircraft's Mach number changes during the 22-s period comprising each data set. These spectra reveal a large change in engine acoustics as the aircraft Mach number increases. At the lowest Mach number of 0.52, the acoustics are characterized by a broad bump centered at 170 Hz. At Mach 0.61 a spike begins to appear in the spectra, and the bump shifts to a lower frequency of

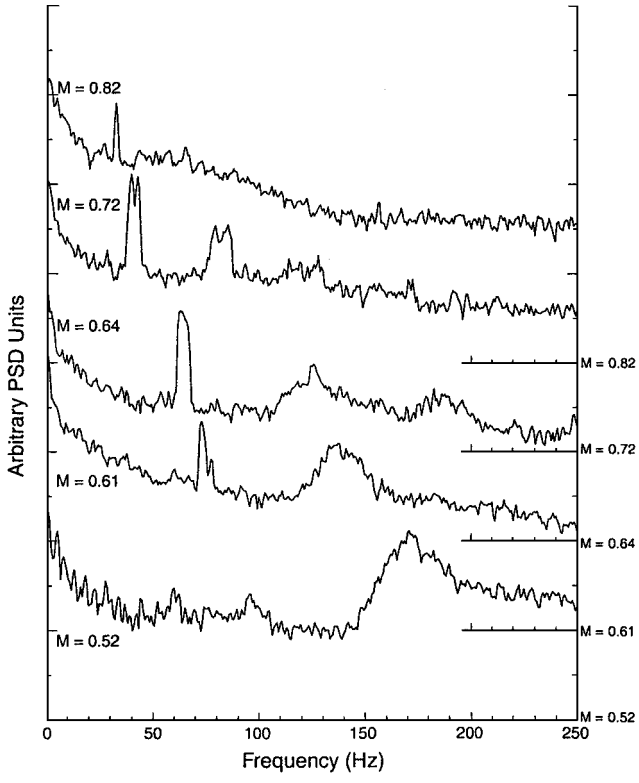

Fig. 12 Spectra of CCA channel for flight 98015a13.

130 Hz. This trend persists at Mach 0.64, where both the spike and the bump are noted to have shifted to a lower frequency when compared to the Mach 0.61 spectra. At Mach 0.72 the spike appears as a double spike, and the bump is poorly defined. The double spike is an artifact because of the sliding-window FFT and results when the spike frequency decreases over the duration of the data set. The trend to lower frequency with increased Mach number persists until Mach 0.82, at which point only the spike is evident. The spectral characteristics do not change significantly for Mach numbers between 0.82 and 0.84. The spectra in Fig. 12 reveal a dependency between the flight Mach number and the frequency of the spike. This dependency is explored further in the next section.

IV. Noise Characterization

The data presented in the preceding section were collected during a limited number of focused flight-test experiments involving both CCA and microphone measurements. In addition to these limited data sets, the atmospheric characterization group at AFRL has collected an extensive database of atmospheric temperature data that includes CCA measurements alone. The preceding section has demonstrated that the temperature fluctuation data contain information regarding engine acoustics. Furthermore, these data were collected under full-scale nonlaboratory conditions. Consequently, the data represent an opportunity to characterize the relationship between the frequency and amplitude of the engine noise as a function of flight speed and altitude. This was accomplished by recording the peak amplitude and frequency of the spike location from 644 temperature fluctuation PSDs collected over a large range of flight conditions. Unfortunately, engine parameter data were not part of the collected data set, and thus it was not possible to compute the jet exhaust velocity, a parameter that would help in interpreting the engine acoustics.

Figure 13 plots data for the spike amplitude as a function of frequency. As the plot is in PSD units of power vs frequency, it describes the domain to which the spike location was found in all of the collected data. As the frequency of the spike decreases, its amplitude increases until reaching a plateau starting at approximately 60 Hz. The amplitude of the spike is seen to remain relatively constant with further decrease in its frequency. Data at both 39,000 ft (11,887 m) and 43,000 ft (13,100 m) were found to cover the entire domain of

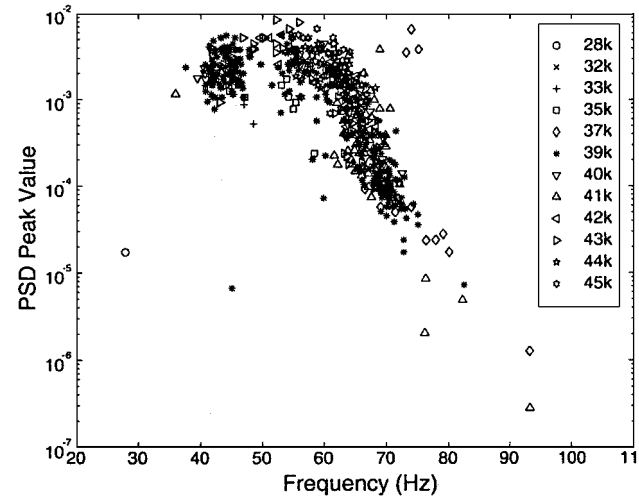

Fig. 13 Spike amplitude vs frequency.

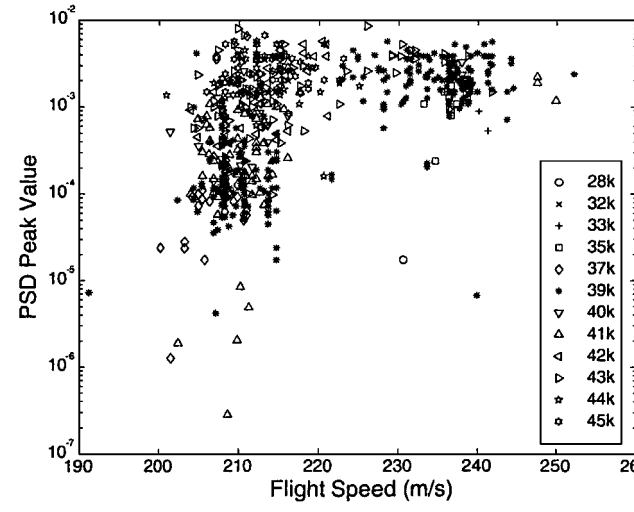

Fig. 14 Spike amplitude vs velocity.

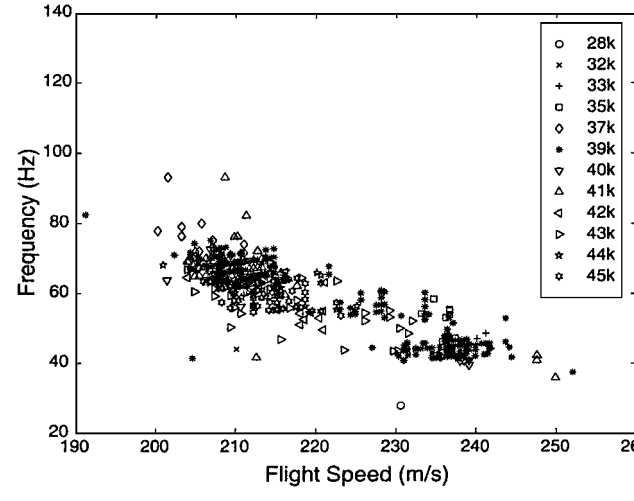

Fig. 15 Frequency of spike as a function of aircraft velocity.

points in the scatter plot, and thus it was concluded that altitude did not have a strong effect on the relationship.

Spike amplitude vs flight speed is shown in Fig. 14, where it is noted that, as flight speed increases, the magnitude of the spike increases up until a plateau value. An increase in flight speed above approximately 215 m/s results in no further increase in the amplitude of the spike. Again, pressure altitude is not a driving factor in the relationship between the magnitude of the spike and flight speed

as data at both 39,000 ft (11,887 m) and 43,000 ft (13,100 m) were found to cover the entire range of values.

When the frequency of the spike is plotted against the flight speed (Fig. 15), a trend is noted where the frequency is found to decrease as the flight speed increases. Similar trends were noted for studies of jet screech frequencies[14] in choked circular jets. These data further support the notion that the source of the spike in the temperature spectra is caused by a resonant interaction between the jet's vortical structures and a quasi-periodic shock cell structure that develops in the jet stream.

V. Conclusions

This paper has presented data to support the claim that non-Kolmogorov features seen in atmospheric temperature data collected from a Grumman Gulfstream II aircraft are caused by the upstream propagation of a nondispersive wave. Spectral analysis techniques, including power spectral density functions, coherence functions, and phase functions, were used to support this claim. The slope of the phase relationship, when measured in units of radians per hertz, can be used to estimate the time delay τ for a wave to propagate upstream between the microphone and constant-current wire. This measure resulted in a time delay of 6.76×10^{-3} s. Knowing the sensor spacing of 0.67 m, the upstream traveling wave speed can be computed to be 98.6 m/s. The difference between the upstream wave speed and the local speed of sound is the local flow speed at the probe mount. From this, the flow speed at the probe mount was estimated to be 85% of the freestream velocity.

The non-Kolmogorov features, having been identified as an upstream propagating wave, are believed to be acoustic in nature and caused by a jet screech interaction between vortical structures in the engines' exhaust streams and a quasi-periodic shock cell structure that develops in the jet stream. This is supported by the fact that other researchers have observed similar power spectral density functions including both spikes and bumps in screech studies for choked convergent nozzles. The Rolls–Royce Spey Mk 511-8 engines on the GII have convergent nozzles. The fact that spectral noise only appears at altitudes above 28,000 ft (8530 m) suggests that at this altitude the jet exhaust becomes choked. Accelerating flight test data revealed large changes in the acoustical character of the engine noise as the flight velocity changed.

Characterization of the spike amplitude and frequency over a large range of flight speeds and altitudes revealed that the spike location was most dependent on flight speed. Increasing flight speed resulted in a decrease in spike frequency and an increase in spike amplitude, reaching a plateau at a flight speed of 215 m/s, where the amplitude was found to remain fixed with further increase in flight speed. The decrease in spike frequency with increasing flight speed has been noted by other researchers studying jet screech in both convergent-divergent and choked convergent nozzles, and this was viewed as being further evidence supporting the claim that the non-Kolmogorov features in the temperature spectra are caused by engine acoustics.

The presence of engine noise in temperature spectra is viewed as a detraction from the perspective of atmospheric data collection. Techniques have been developed to remove the engine noise from temperature spectra and are described in a separate paper.[20] Other filtering techniques have been implemented, mainly consisting of analyzing the spectra at wave numbers below the region where the engine acoustics contaminate the signal, and these methods have proven successful at enabling the quantification of atmospheric temperature fluctuation strength.

Acknowledgments

The authors would like to thank Tom Straiton, Art Harris, Darren Paul, Danny Sutton, and Mike Saslawsky of MetroLaser, Inc., Albuquerque, New Mexico, for being adaptable while preparing for and performing the flight tests.

References

[1]Otten, L. J., Pavel, A. L., Finley, W. E., and Rose, W. C., "A Survey of Recent Atmospheric Turbulence Measurements from a Subsonic Aircraft," AIAA Paper 81-0298, Jan. 1981.

[2]Rose, W. C., and Otten, L. J., "Airborne Measurements of Atmopheric Turbulence," *Aero-Optical Phenomena*, Vol. 80, Progress in Astronautics and Aeronautics, AIAA, New York, 1982, pp. 325–337.

[3]Masson, B., Scruggs, B., Hayes, M., Wissler, J., Bishop, K., and Kyrazis, D., "Airborne Measurement of Tropopausal Temperature Fluctuations," AIAA Paper 96-0265, Jan. 1996.

[4]Jumper, G. Y., Beland, R. B., Roadcap, J. R., and Cote, O. R., "Effect of Compressible Flow on Perceived Temperature Fluctuations Measured by a Moving Sensor," *AIAA Journal*, Vol. 37, No. 12, 1999, pp. 1609–1616.

[5]Hugo, R. J., Nowlin, S. R., Hahn, I. L., Bishop, K. P., and McCrae, K., "Aircraft-Based in-situ Calibration of a Hot-Wire Anemometer in a Compressible Flow," *Airborne Laser Advanced Technology II*, *Proceeding of SPIE*, Vol. 3706, edited by T. D. Steiner and P. H. Merritt, Society of Photo-Optical Instrumentation Engineers (International Society for Optical Engineering), Bellingham, WA, 1999, pp. 54–67.

[6]Wisniewski, C., Scruggs, B., Masson, B., Kyrazis, D., and Truman, C. R., "Calibration of Constant Current Anemometer Probes for Aircraft Based Atmospheric Turbulence Measurements," AIAA Paper 95-1985, June 1995.

[7]Hinze, J. O., *Turbulence*, 2nd ed., McGraw–Hill, New York, 1975, p. 228.

[8]Frisch, U., *Turbulence, The Legacy of A. N. Kolmogorov*, Cambridge Univ. Press, Cambridge, England, U.K., 1995, p. 62.

[9]Nastrom, G. D., and Gage, K. S., "A Climatology of Atmospheric Wavenumber Spectra of Wind and Temperature Observed by a Commercial Aircraft," *Journal of the Atmospheric Sciences*, Vol. 42, No. 9, 1985, pp. 950–960.

[10]Hugo, R. J., Nowlin, S. R., McCrae, K. A., Hahn, I. L., and Bishop, K. P., "Shedding Characteristics of a Low Aspect Ratio Probe Mount in Subsonic Flow," AIAA Paper 98-2831, 1998.

[11]Seiner, J. M., "Advances in High Speed Jet Aeroacoustics," AIAA Paper 84-2275, 1984.

[12]Norum, T. D., "Screech Supression in Supersonic Jets," *AIAA Journal*, Vol. 21, No. 2, 1983, pp. 235–240.

[13]Tam, C. K. W., Seiner, J. M., and Yu, J. C., "Proposed Relationship Between Broadband Shock Associated Noise and Screech Tones," *Journal of Sound and Vibration*, Vol. 110, No. 2, 1986, pp. 309–321.

[14]Powell, A., Umeda, Y., and Ishii, R., "Observations of the Oscillation Modes of Choked Circular Jets," *Journal of the Acoustical Society of America*, Vol. 92, No. 5, 1992, pp. 2823–2836.

[15]Bendat, J. S., and Piersol, A. G., *Random Data, Analysis and Measurement Procedures*, 2nd ed., Wiley, New York, 1986, p. 137.

[16]Piersol, A. G., "Use of Coherence and Phase Data Between Two Receivers in Evaluation of Noise Environments," *Journal of Sound and Vibration*, Vol. 56, No. 2, 1978, pp. 215–228.

[17]Bendat, J. S., and Piersol, A. G., *Engineering Applications of Correlation and Spectral Analysis*, 2nd ed., Wiley, New York, 1993, p. 170.

[18]Goldstein, M. E., *Aeroacoustics*, McGraw–Hill, New York, 1975, pp. 98–105.

[19]Seiner, J. M., Manning, J. C., and Ponton, M. K., "Dynamic Pressure Loads Associated with Twin Supersonic Plume Resonance," *AIAA Journal*, Vol. 26, No. 8, 1988, pp. 954–960.

[20]Hugo, R. J., Nowlin, S. R., Hahn, I. L., Eaton, F. D., and McCrae, K. A., "Application of Acoustic Noise Removal Methods to Aircraft-Based Atmospheric Temperature Measurement," AIAA Paper 99-3622, 1999.

J. P. Gore
Associate Editor